Applied Surface Science 576 (2022) 151879

Contents lists available at ScienceDirect

Applied Surface Science

journal homepage: www.elsevier.com/locate/apsusc

Full Length Article

CuCo-Cu@CoCH stamen-like nanoarray prepared by co-reduction for electrochemical detection of hydrogen peroxide

Ning Han [a], Shiyu Hu [a], Liying Zhang [a], Shasha Yi [a], Zongtao Zhang [a], Yu Wang [a], Ying Zhou [a], Deliang Chen [a], Yanfeng Gao [b]

[a] School of Materials Science and Engineering, Zhengzhou University, No. 100 Science Avenue, Zhengzhou 450100, Henan, China
[b] School of Materials Science and Engineering, Shanghai University, No. 333 Nanchen Road, Shanghai 200444, China

ARTICLE INFO

Keywords:
Electrochemical sensor
Electroanalysis
Hydrogen peroxide
Co-reduction
Nanoarray

ABSTRACT

Accurate and convenient detection of H_2O_2 is of great significance for the diagnosis and treatment to some diseases. Herein, a unique stamen-like CuCo-Cu@Co$(CO_3)_{0.5}$(OH) (defined as CuCo-Cu@CoCH) nanoarray was fabricated by cation exchange and co-reduction for electrochemical detection of H_2O_2. The nanostructure with large electrochemical surface area can adsorb H_2O_2 efficiently, while the Cu@CoCH nanowire offers a high-way for electron transfer, and the CuCo nanoparticle possesses high activity for H_2O_2 reduction. Hence, the CuCo-Cu@CoCH nanoarray performs excellently as a electrochemical H_2O_2 sensor with a high sensitivity of 3570 μA mM^{-1} cm^{-2} (1 μM to 100 μM) and 3290 μA mM^{-1} cm^{-2} (100 μM to 2000 μM), a fast response time (< 1.5 s), a low detection limit (0.97 μM, S/N = 3) and superior selectivity, stability. Furthermore, the nanoarray shows promising electrochemical activity for real-time detection of H_2O_2 released from HepG2 human liver cancer cells. This work offers a novel material as electrochemical sensor to H_2O_2 with enhanced performance, and shows a new solution to prepare nanostructure of alloy.

1. Introduction

Hydrogen peroxide (H_2O_2) is an important product of human metabolism, which can kill invading pathogens and promote wound healing and repair process in an appropriate amount [1–3]. However, under excessive pressure, cells would produce large amounts of hydrogen peroxide, which can cause apoptosis, necrosis and autophagy, and finally trigger oxidative stress – this is an important mechanism of many liver injury diseases [4–6]. Therefore, timely and accurate detection of H_2O_2 is of great significance for disease prevention [7,8]. Common detection methods of H_2O_2 include titration [9], spectroscopy [10], colorimetry [11], chemiluminescence detection [12], electrochemical detection [13,14] and so on, among which, electrochemical detection is widely concerned because of its convenience, high accuracy and low-priced [15–20]. While much attention is paid on non-enzyme electrode in electrochemical detection, which is more stable and easy to preserve than enzymic one.

Hydrogen peroxide can be reduced by superoxide dismutase (SOD) in human body, and the most common enzyme is Cu–Zn SOD, in which Cu is the main active center [21,22]. Therefore, copper-based materials have promising catalytic reduction activity for hydrogen peroxide and can be used for its detection [23–25]. Co based materials are also widely used in the electrochemical detection of hydrogen peroxide due to its abundant variable valence. Cu and Co composites can form the redox cycle of Co (III)/Co (II) and Cu (II)/Cu (I) electron pairs, accelerate the interfacial electron transfer process, and further improve the catalytic reduction ability of hydrogen peroxide [26], for instance, various nanostructures of $CuCo_2O_4$ have been reported for hydrogen peroxide detection [27–30].

Composites of metal compound and metal nanoparticle/quantum dot usually have excellent performance in (photo) electrochemical catalysis, sensing and other fields due to the high activity of compounds and the high conductivity of metal particles [20,31–38]. And among the synthesis methods, in situ synthesis is an effective method to accelerate electron transfer as it ensures the close contact between metal particles and compounds [39]. For example, as a photocatalytic material, BiOX (x = Cl, I, Br) could be partially reduced to Bi in situ by adding appropriate amount of glucose in the preparation process. The reduced Bi forms SPR effect on the surface of BiOX, which accelerates the separation of photogenerated electron-hole and effectively improves the photocatalytic activity [40]. It has also been reported that Co–CoO Janus catalyst was prepared by one-step solution, which can effectively utilize the activity

E-mail address: zhangliying@zzu.edu.cn (L. Zhang).

https://doi.org/10.1016/j.apsusc.2021.151879
Received 2 August 2021; Received in revised form 24 October 2021; Accepted 9 November 2021
Available online 12 November 2021

of the two materials and form Mott-Schottky heterojunction between Co and CoO, thus accelerate the electron flow and improve the electrocatalytic activity [41]. Due to the synergistic geometric and electronic effect, bimetallic particles usually exhibit better catalytic activity than the monometallic particle, such as Cu-Ni, Cu-Co etc. [42,43]. However, many metal compounds are not easy to be reduced under mild conditions, furthermore, the metal nanoparticles are inclined to aggregate and the activity would decrease, so the synthesis of metal/metal compound composite is worthy of further study.

In this paper, a CuCo-Cu@CoCH composite nanoarray was synthesized by a co-reduction method, in which CuCo alloy nanoparticles were loaded on the top of Cu@CoCH nanowires, forming a structure similar to stamen. $Cu(OH)_2$ can be reduced to Cu by $NaBH_4$, but CoCH cannot be reduced at the same condition, however, if there exists Cu, it can be reduced in the form of CuCo alloy. The mechanism of this co-reduction reaction was systematically analyzed, and the reaction was further extended to CuNi system. The as-prepared CuCo-Cu@CoCH composite showed excellent performance in the detection of hydrogen peroxide with a sensitivity of 3570 μA mM^{-1} cm^{-2} (1 μM–100 μM), 3290 μA mM^{-1} cm^{-2} (100 μM–2000 μM), an outstanding selectivity and reproducibility, and could be used for the real-time detection of hydrogen peroxide released from HepG2 human liver cancer cells.

2. Result and discussion

2.1. Characterization of CuCo-Cu@CoCH nanoarray

As shown in Fig. 1a, the preparation procedure for the stamen-like CuCo-Cu@CoCH nanoarray was composited with hydrothermal, cation exchange and co-reduction. The $Co(CO_3)_{0.5}(OH)$ (CoCH) nanowire array was directly grown on Ni foam (NF) substrate by hydrothermal method, which was then immersed in Cu^{2+} solution to obtain $Cu(OH)_2$@CoCH by cation exchange. Finally, stamen-like CuCo-Cu@CoCH nanoarray was obtained by reducing $Cu(OH)_2$@CoCH with $NaBH_4$.

It could be seen in the SEM images that the CoCH nanowires were uniformly and neatly arranged on the NF substrates (Fig. 1b), after cation exchange, nanoparticles appeared on top of the nanowires (Fig. 1c). Finally, after reduction with $NaBH_4$, a stamen-like structure could be seen with neatly arranged nanowires and nanoparticles scattered above (Fig. 1d). In addition, electrodes that exchanged with Cu^{2+} for different times were prepared to understand the evolution of the microstructure morphology. As shown in Fig. S2a-b, there were only a few CuCo alloy particles on the CoCH nanowires when the immersion time was 20 min. However, when immersion time extended to 90 min, samples were peeled off from the NF substrates, so 60 min was chosen as the optimal cation exchange time and subsequent characterization.

To investigate the composition of the as-prepared samples, XRD and FT-IR tests were carried out. In the XRD spectrum, due to the shielding effect of NF, there was only peaks for NF of the CoCH sample (the blue line in Fig. 1e), however, new peaks at 17.5°, 33.8°, 35.5° and 39.5° appeared as the samples scraped off from the NF, which belonged to (020), (221), (040) and (231) of CoCH, respectively (Fig. S3) [44], confirming the formation of CoCH. The XRD pattern of the sample after cation exchange (the black line in Fig. 1e) exhibited peaks at 16.7°, 33.9° and 39.9°, which were corresponded well to (020), (002) and (130) planes of $Cu(OH)_2$ (JCPDS no. 72-0140) [45], respectively,

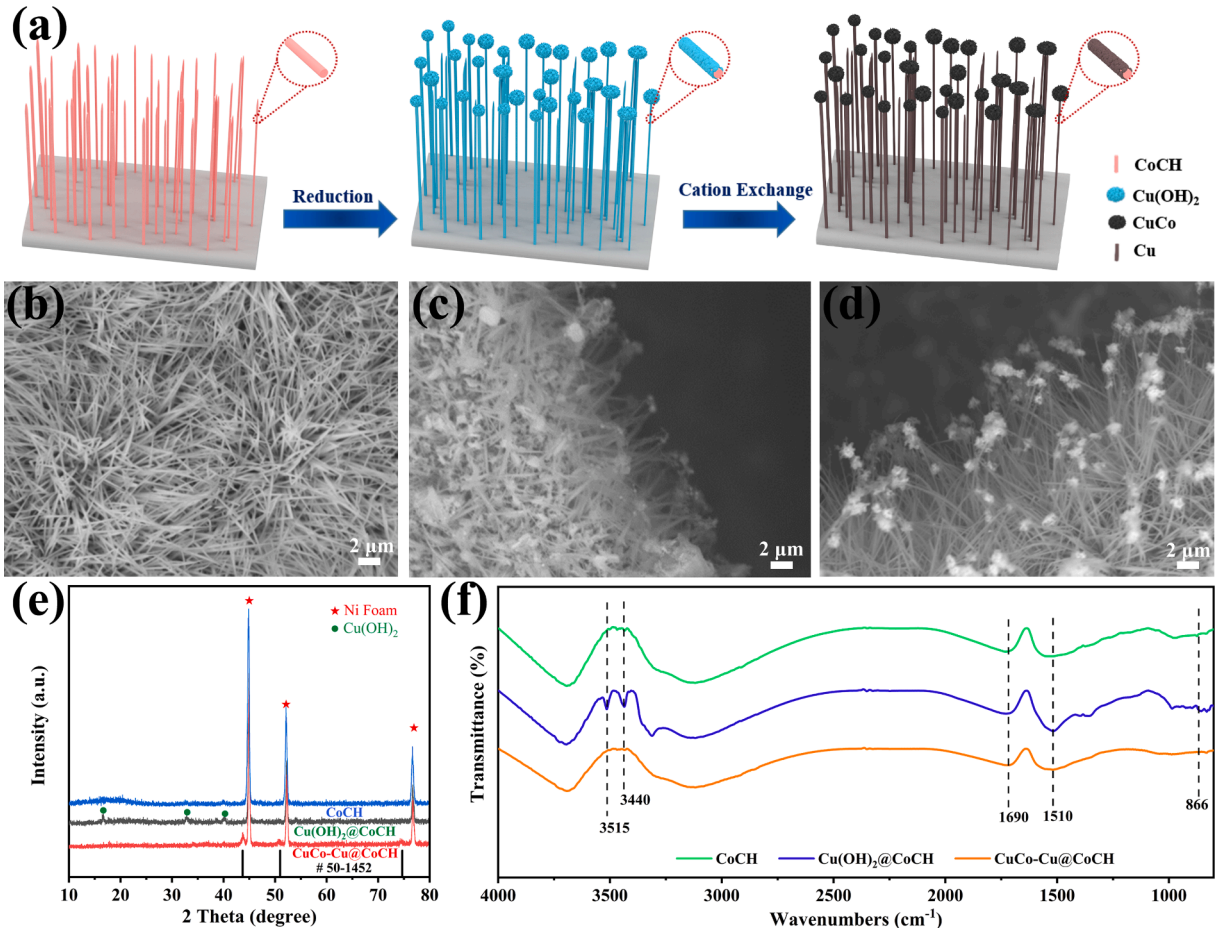

Fig. 1. (a) Schematic illustration of the formation process of CuCo-Cu@CoCH nanoarray; SEM images of (b) CoCH nanowires, (c) $Cu(OH)_2$@CoCH nanoarray, (d) CuCo-Cu@CoCH nanoarray; (e) XRD patterns of CoCH, $Cu(OH)_2$@CoCH and CuCo-Cu@CoCH; (f) Fourier transform infrared (FT-IR) spectra of CoCH, Cu $(OH)_2$@CoCH and CuCo-Cu@CoCH.

revealing the partly exchange from CoCH to $Cu(OH)_2$. The peaks for $Cu(OH)_2$ disappeared in the spectrum after reduction (the red line in Fig. 1e), and new peaks at 43.7°, 50.9° and 74.6° belonging to (020), (002) and (130) plane of CuCo (JCPDS no. 50-1452) appeared [46], indicating the transform from $Cu(OH)_2$ to CuCo. In the FT-IR spectrum of CoCH nanowire array (green line in Fig. 1f), there were two faint peaks at 3440 cm^{-1} and 3515 cm^{-1} for M—OH stretching vibration, two peaks at 1690 cm^{-1} and 1510 cm^{-1} for H—O—H vibration, and a peak at 866 cm^{-1} for CO_3^{2-} vibration [47,48]. Then the peaks for M—OH stretching vibration increased significantly after Cu^{2+} exchange (purple line in Fig. 1f), indicating the formation of $Cu(OH)_2$, and after reduction with $NaBH_4$, the two peaks decreased dramatically (orange line in Fig. 1f), demonstrating the decomposition of $Cu(OH)_2$ and CoCH.

TEM further revealed the morphology and composition of CuCo-Cu@CuCo. As was shown in the low-resolution TEM image (Fig. 2a), there was a stamen-like morphology of the nanoarray. High-resolution TEM images (Fig. 2b-c) displayed lattice fringes of 0.265 nm and 0.228 nm corresponding to (221) and (231) planes of CoCH, and 0.207 nm assigned to the (111) plane of CuCo [49,50]. Then the elemental mapping images clearly revealed the composition of the CuCo-Cu@CuCo nanostructure (Fig. 2d-g). Cu and Co were distributed in the nanowire and nanoparticle, while O elemental was only found in the nanowire, revealing the nanoparticle was CuCo alloy. Furthermore, Cu was almost distributed in the whole nanowire, and Co, O only existed in the inner of the nanowire, demonstrating the Cu@CoCH composition of the nanowire.

XPS spectrum was tested to characterize the surface composition and valence state of the CuCo-Cu@CoCH nanoarray. C, Ni, Cu, Co and O appeared in the XPS full spectrum (Fig. 3a), which was consistent with the elemental mapping results in Fig. 2d-e. In the high-resolution C 1s spectra of Fig. S4, three peaks at 284.5 eV, 286.2 eV, and 288.9 eV could be observed, which were attributed to the presences of C—C, C—O and C═O species of CoCH. As shown in Fig. 3b, The Cu 2p spectra could be deconvoluted into five prominent peaks at 932.2 eV, 934.4 eV, 942.6 eV, 952.2 eV and 954.4 eV, while the sharp peaks of 932.2 eV and 952.2 eV corresponded to Cu $2p_{3/2}$ of zero-valent, which might be derived from CuCo alloy and metallic Cu, the broad peaks of 934.4 eV and 954.4 eV corresponded to Cu $2p_{1/2}$ of Cu(II), which might be caused by the unreduced Cu^{2+} in CuCo-Cu@CoCH or metallic Cu oxidized in the air, and the peak of 942.6 eV was a satellite peak. After deconvolution, the Co 2p spectra in Fig. 3c was fitted with five peaks. Peaks at 780.9 and 796.8 eV were assigned to Co(II) $2p_{3/2}$ and $2p_{1/2}$, and the 775.6 eV peak belonged to zero-valent Co in the metallic state. As for O 1s spectra in Fig. 3d, the peak at 531.1 eV and 532.3 eV possibly stated the existence of M—OH (Co—OH) and O—C═O, respectively, and the peak at 533.9 eV indicated the presence of adsorbed water [46,49–52]. The results further confirm the formation of CuCo-Cu@CoCH.

2.2. Electrochemical performance of CuCo-Cu@CoCH

CV measurements were performed in 0.1 M PBS in the absence and presence of 1000 μM H_2O_2 to verify the activity of CuCo-Cu@CoCH electrode for H_2O_2 detection. As shown in Fig. 4a, there was a reduction peak at −0.25 V (vs. SCE) and a rather weak oxidation peak at −0.1 V without H_2O_2. This pair of redox peaks might be attributed to the redox reaction of CuCo [26]. The reduction peak increased observably after addition of 1000 μM H_2O_2, suggesting that H_2O_2 was involved in the reaction, so the potential near the reduction peak was chosen for the following tests.

To investigate the effect of different parts of the nanocomposite, CVs were recorded for the CoCH(Fig. S5a); Cu@CoCH(Fig. S5b); Co@CoCH (Fig. S5c),CuCo/NF (Fig. S5d) and CuCo-Cu@CoCH (Fig. S5e) in 0.1 M PBS (pH 7.0) with and without 1.0 mM H_2O_2. And by comparison between the current differences at potential between −0.20~−0.40 V, it could be clearly seen that the CuCo-Cu@CoCH electrode exhibited the best activity to H_2O_2 at −0.25 V (Fig. S5f).

CVs are recorded for the CoCH and $Cu(OH)_2$@CoCH electrodes in 0.1 M PBS with and without H_2O_2 (Fig. S6a). The catalytic peak current of H_2O_2 recorded for the CuCo-Cu@CoCH electrode was 1.07 A at −0.25 V, which was 7.1 and 8.9 times higher than those of the CoCH and $Cu(OH)_2$@CoCH electrodes, respectively. And the sensitivity of H_2O_2 detection in the range of 100–700 μM for CuCo-Cu@CoCH (3290 μA mM^{-1} cm^{-2})was much larger than that of $Cu(OH)_2$@CoCH (257 μA mM^{-1} cm^{-2})and CoCH (29 μA mM^{-1} cm^{-2}) (Fig. S6b-d).

Larger electrochemical surface area (ESCA) meant facile interfacial charge transfer, so it was important to the detection of trace amounts of chemical species [53,54]. The double-layer capacitance (C_{dl}), which was in proportion with the ESCA of the electrode, could be obtained by plotting the ΔJ /2 with the scan rate (Fig. S7a-d), where ΔJ represented the difference between anodic and cathodic current under the same potential. The ESCA of CuCo-Cu@CoCH (12.81 mF cm^{-2}) was much larger than that of $Cu(OH)_2$@CoCH (1.23 mF cm^{-2}) and CoCH (0.24 mF

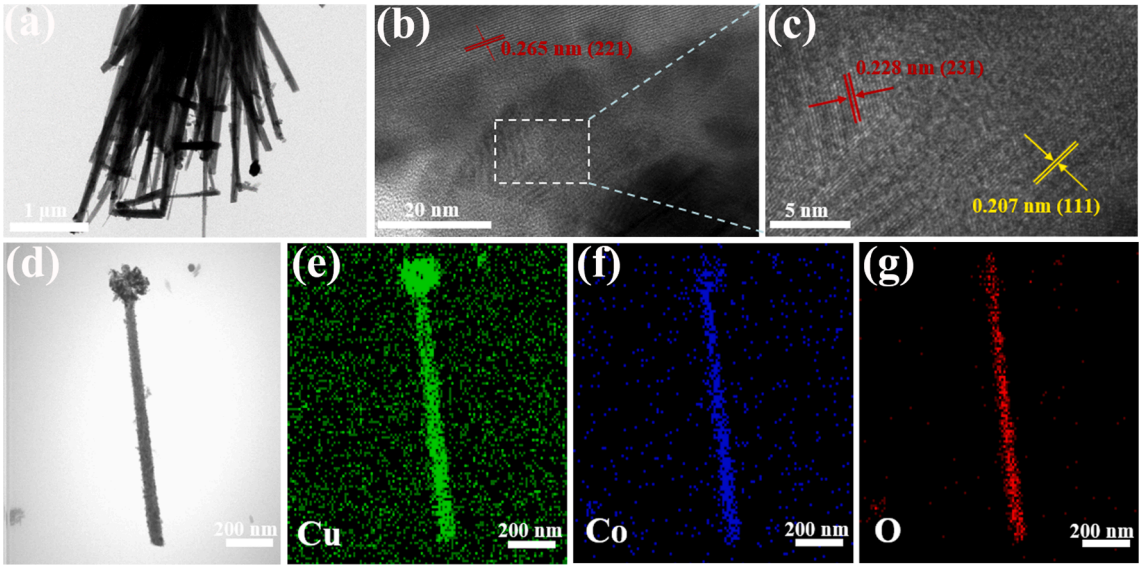

Fig. 2. (a) TEM image of the CuCo-Cu@CoCH; (b, e) HRTEM images of the CuCo-Cu@CoCH nanoarray; (d-g) elemental mapping images of the CuCo-Cu@CoCH nanoarray.

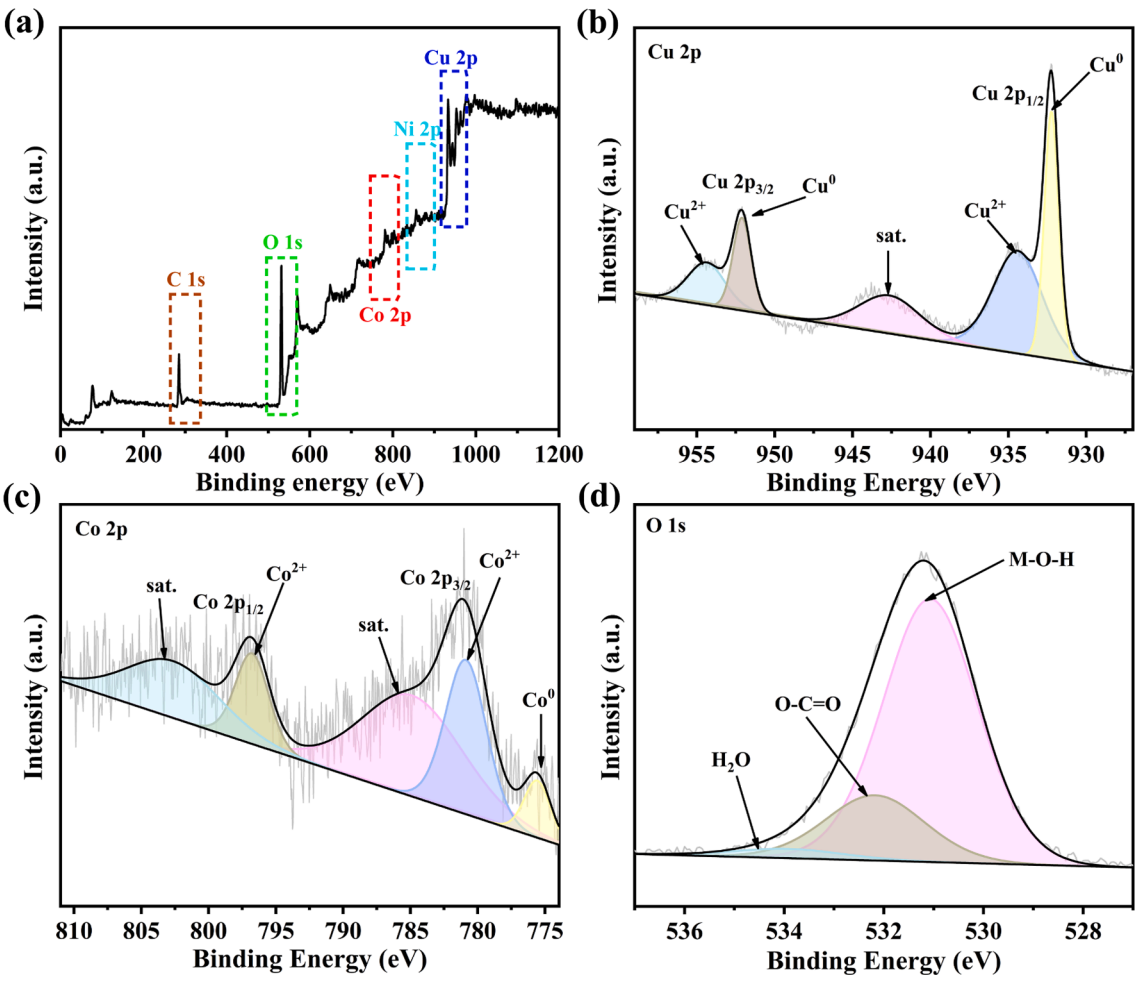

Fig. 3. (a) XPS survey scan of the CuCo-Cu@CoCH; XPS spectra of (b) Cu 2p, (c) Co 2p and (d) O 1s in CuCo-Cu@CoCH nanoarray.

cm^{-2}), demonstrating that the CuCo-Cu@CoCH electrode had larger ESCA to participate in the reaction. Then CV curves of CuCo-Cu@CoCH under different H_2O_2 concentrations were tested (Fig. 4b), in which the reduction peak at −0.25 V increased in proportion with the of H_2O_2 concentration from 200 μM to 1000 μM. All the results indicated that the CuCo-Cu@CoCH electrode might be a promising H_2O_2 sensor.

To investigate the adsorption and activation behavior of H_2O_2 on CuCo-Cu@CoCH electrode, CV curves with different scan rates were tested under different H_2O_2 concentrations. The CV curves at low H_2O_2 concentration (800 μM) was shown in Fig. 4c, from which it could be found that there was a perfect linear relationship between the reduction peak current and scan rate (inset in Fig. 4c), suggesting an adsorption-controlled process of H_2O_2 reduction on the electrode [55,56]. However, reduction peak current was proportional to the square root of scan rate at high H_2O_2 concentration (2000 μM) (Fig. 4d), demonstrating a typical diffusion-controlled reaction [57–59]. The different adsorption and activation behavior of H_2O_2 under different concentrations might lead to different linear regions in the following detection [60], which was further verified in Fig. 5c.

2.3. Amperometric measurement of H_2O_2

To find the optimal applied potential, amperometric tests with successive addition of H_2O_2 under different potentials were carried out (Fig. 5a). The electrochemical response increased with the applied potential stepped from −0.20 V to −0.25 V, but as the potential increased to −0.28 V, the current response began to decrease. As shown in the calibration curve in Fig. 5b, the current response at −0.25 V had the largest slope, so −0.25 V was chosen as the optimal applied potential in H_2O_2 detection.

As shown in Fig. S8a, amperometric measurements of CuCo-Cu@CoCH with different exchange times were performed at −0.25 V in 0.1 M PBS solution with the successive addition of 100 μM H_2O_2. Compared with the electrode with 20 min and 40 min, the CuCo-Cu@CoCH electrode with exchange time of 60 min had a more obvious response to H_2O_2, however, with the further increase of the exchange time, the response decreased, the electrode with 80 min exhibited a little weaker response than the 60 min one, and the 90 min one showed a much weaker response. Converted into the linear relationship between H_2O_2 concentration and response current (Fig. S8b), CuCo-Cu@CoCH electrode had the largest slope when the cation exchange time was 60 min. The results were in consistent with the morphology in SEM images in Fig. 1d and Fig. S2a-b, and CuCo-Cu@CoCH electrode with exchange time of 60 min was selected for the subsequent testing.

Fig. 5c showed the amperometric curve of CuCo-Cu@CoCH at −0.25 V with successive addition of H_2O_2 every 60 s. With the addition of H_2O_2, the CuCo-Cu@CoCH had a fast response time, as shown in Fig. S9 the steady current response could be reached within 1.5 s. Furthermore, the calibration curve between H_2O_2 concentration and the current response was shown in Fig. 5d. The linear relationship at 1 μM–100 μM could be expressed as I (mA cm^{-2}) = −3.57C (mM) −0.20459 (R^2 = 0.9983), and I (mA cm^{-2}) = −3.29C (mM) −0.32722 (R^2 = 0.9989) at 100 μM–2000 μM, where I represented the current density, C represented the H_2O_2 concentration and the slope indicated the sensitivity to H_2O_2 concentration, so the sensitivity was 3570 μA mM^{-1} cm^{-2} (1

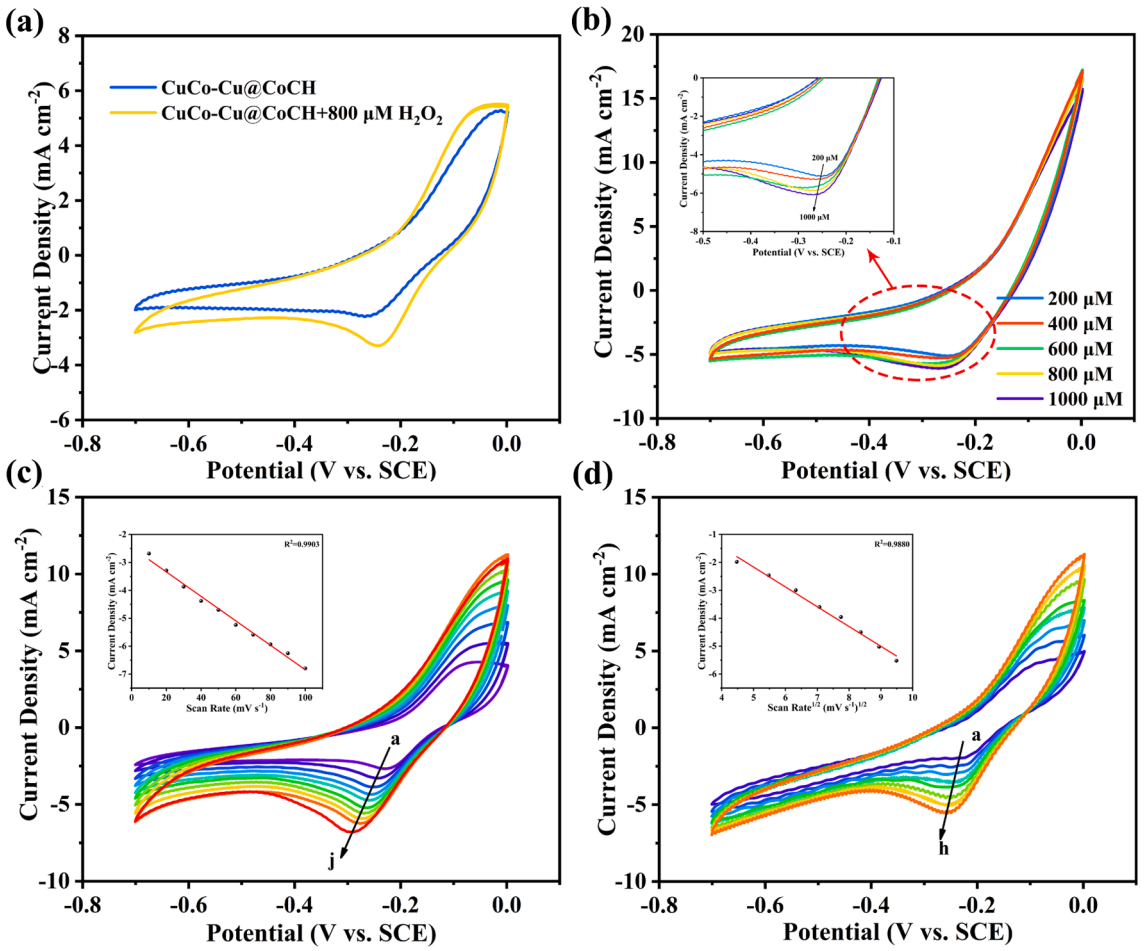

Fig. 4. (a) CV curves of the CuCo-Cu@CoCH electrode in N_2-saturated 0.1 M PBS solution (PH = 7) in the absence and presence of 1000 μM H_2O_2 (scan rate: 20 mV s^{-1}); (b) CV curves of the CuCo-Cu@CoCH electrode in 0.1 M PBS solution with different H_2O_2 concentrations (scan rate: 20 mV s^{-1}), and inset is the enlargement of the CV curve from −0.1 to −0.5 V; (c) CV curves of the CuCo-Cu@CoCH electrode at different scanning rates (10–100 mV s^{-1}, a–j) in 800 μM H_2O_2, and inset is the relationship between reduction peak current density and scan rate; (d) CV curves of the CuCo-Cu@CoCH electrode at different scanning rates (20–90 mV s^{-1}, a–h) in 2000 μM H_2O_2, and inset is the relationship between reduction peak current density and the square root of scan rate.

μM–100 μM) and 3290 μA mM^{-1} cm^{-2} (100 μM–2000 μM), respectively. The lowest detection limit (LOD) was calculated to be 0.97 μM (LOD = 3σ/N, σ was the standard deviation of background current while N was the sensitivity).

Table 1 displayed materials reported recently for the electrochemical detection of H_2O_2 for comparison, among which the CuCo-Cu@CoCH electrode as prepared presented an outstanding electrochemical performance for H_2O_2 with high sensitivity and low LOD, which could be attributed to the unique stamen-like structure.

2.4. Selectivity, reproducibility, and stability of CuCo-Cu@CoCH

To analyse the selectivity of CuCo-Cu@CoCH electrode, 1000 μM sodium chloride (NaCl), potassium chloride (KCl), ammonium chloride (NH_4Cl), sodium nitrite ($NaNO_2$), uric acid (UA), ascorbic acid (AA), glucose, saccharose and 100 μM H_2O_2 were successively added to 0.1 M N_2-saturated PBS at −0.25 V. As shown in Fig. 6a-b, the CuCo-Cu@CoCH electrode had a negligible response to the interferes even though they were 10 times more concentrated than H_2O_2. The current responses to NaCl, KCl, NH_4Cl, $NaNO_2$, UA, AA, glucose and saccharose were calculated to be only 4.1%, 6.1%, 3.3%, 2.2%, 4.3%, 3.6%, 3.7% and 4.3% relative to H_2O_2, demonstrating that the excellent selectivity of the stamen-like CuCo-Cu@CoCH electrode for the detection of H_2O_2.

Reproducibility and stability should also be considered in the actual application of the sensor. To investigate the reproducibility of the CuCo-Cu@CoCH electrode, amperometric response was used to investigate the electrochemical signal of the CuCo-Cu@CoCH electrode with the addition of 100 μM H_2O_2. The relative standard deviation (RSD) of the current signal was only 4.7% for 8 electrodes (Fig. 6c), suggesting that the CuCo-Cu@CoCH electrode possessed favorable reproducibility.

Moreover, the stability of the CuCo-Cu@CoCH electrode was tested by recording the current signal with addition of 100 μM H_2O_2 during a week. The RSD was 3.7% of the different days (Fig. 6d), moreover, the morphology of CuCo-Cu@CoCH was little changed after the stability test (Fig. S10a-b), demonstrating that the CuCo-Cu@CoCH electrode had superior stability.

2.5. Measuring H_2O_2 secreted from human liver cancer HepG2 cells

To investigate the effectiveness of practical application of CuCo-Cu@CoCH sensor in real samples, amperometric measurement was carried with CuCo-Cu@CoCH electrode to detect H_2O_2 released from HepG2 cells at −0.25 V (vs. SCE) in N_2-saturated 0.1 M PBS solution. As was shown in Fig. 7, there was a negligible current change on the electrode after injection of 5 mM ascorbic acid (AA) into the 0.1 M PBS (red line). However, after addition of the 5 mM AA solution into the 0.1 M PBS solution with HepG2 cells (blue line), an obvious current response could be found. The current signal was recorded to be 0.109 mA, corresponding to 29 μM H_2O_2 released from the HepG2 cells.

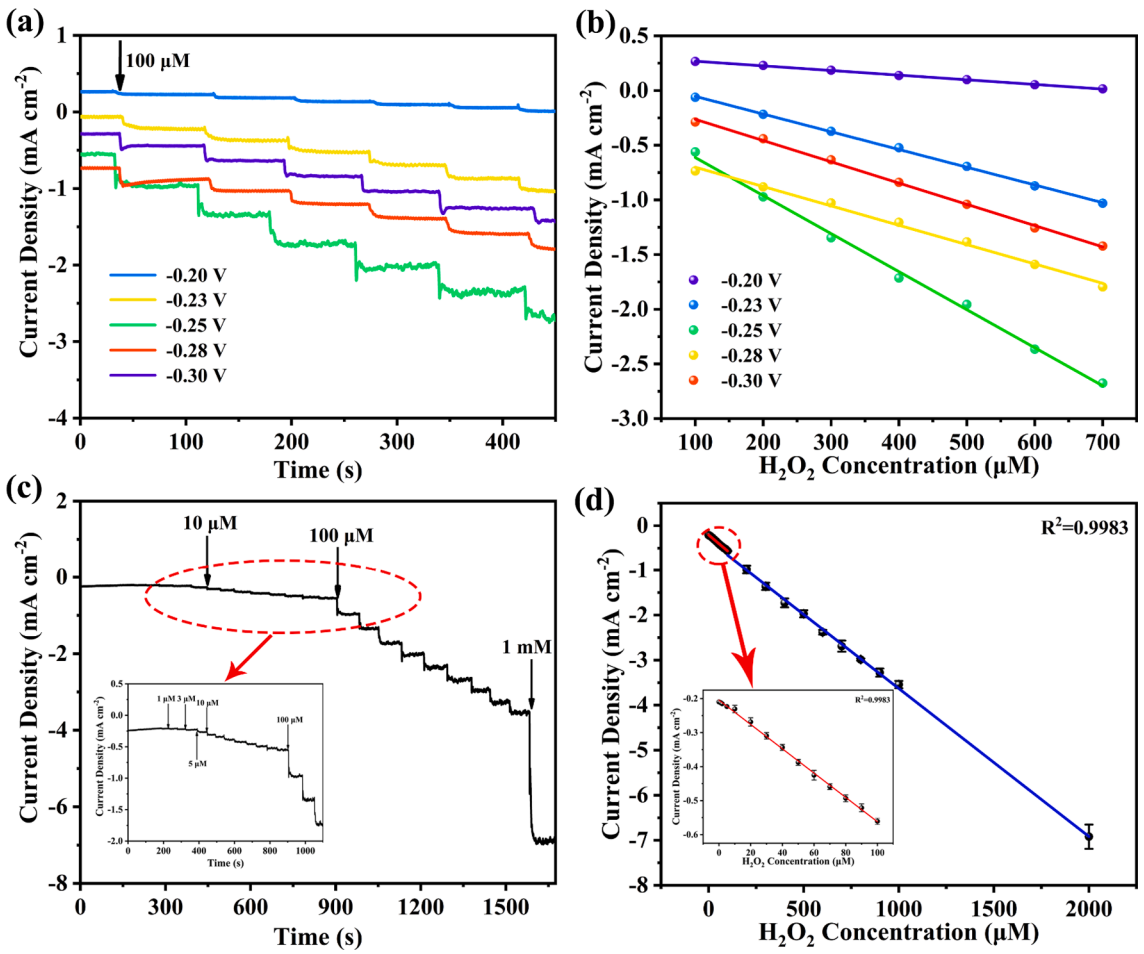

Fig. 5. (a) Amperometric responses of CuCo-Cu@CoCH electrode at different potentials in 0.1 M PBS solution with the successive addition of 100 μM H_2O_2; (b) The relationship between response current density and H_2O_2 concentration of CuCo-Cu@CoCH at various potentials in 0.1 M PBS solution; (c) Amperometric responses of the CuCo-Cu@CoCH electrode to the successive addition of H_2O_2 in 0.1 M PBS at −0.25 V (vs. SCE). The inset shows the low concentration of H_2O_2 (1–40 μM); (d) The linear relationship between current density and H_2O_2 concentration of CuCo-Cu@CoCH at −0.25 V in 0.1 M PBS solution. The inset shows the H_2O_2 concentration from 1 to 100 μM.

Table 1
Comparison of the performance of different H_2O_2 sensors.

Electrode materials	Linear range (μM)	Sensitivity (μA mM^{-1} cm^{-2})	Detection limit (μM)	Ref
Meso-C/ZnO	50–981	46.48	6.25	[61]
CuO NWs/3D-Cu foam	1–1000	8870	0.98	[62]
CuO/GCE	5–180	8.6	1.6	[63]
ITO-rGO-AuNPs	25–3000	64.1	6.65	[64]
Co_3O_4/rGO/GCE	15–675	1.14	2.4	[65]
NiO-NSs/CF-1801/	200–3750	23.30	0.013	[20]
HRP/HAuDE	3–400	/	1.5	[66]
nanoporous gold	10–1800	/	0.6	[67]
$CoFe_2O_4$ @CdSeQDs/RIF/GC	7–145 145–1430	143.01 28.67	0.38	[68]
CuCo-Cu@CoCH	1–100 100–2000	3570 3290	0.97	This work

2.6. Formation mechanism of CuCo-Cu@CoCH

Compared with other reports on $NaBH_4$ reduction, a much lower concentration of $NaBH_4$ was used in this paper. CoCH could not be reduced to Co under this solution, as shown in SEM images (Fig. S11a-b), the morphology of CoCH nanowire array before and after $NaBH_4$ reduction had almost no change. Moreover, the XRD pattern in Fig. S11c also showed no new phase after $NaBH_4$ reduction, indicating that pure CoCH nanowire could not be reduced in low concentration $NaBH_4$ solution. On the contrary, $Cu(OH)_2$ nanowire can be directly reduced to Cu by low concentration $NaBH_4$ solution [45,69].

Cu(II) can be reduced to the metallic state with a relatively mild reductant such as NH_3BH_3, while Co(II) cannot. However, if there is a small amount of Cu^{2+} in CoO, Cu^{2+} could react with NH_3BH_3 to form Cu–H active intermediate, which can help further reduce part of CoO to Co and form CuCo alloy [51,70].

In this work, $Cu(OH)_2$ was formed on the surface and tip of CoCH nanowire by cation exchange. In the presence of Cu^{2+}, the tip of CoCH nanowire, which was the most active area, was reduced simultaneously by low concentration $NaBH_4$ solution to form CuCo alloy nanoparticles, while the $Cu(OH)_2$ wrapped outside the CoCH was reduced to Cu, and finally formed CuCo-Cu@CoCH composite nanoarray structure.

This co-reduction process also occurred on nickel hydroxide materials. $Cu(OH)_2$-$Ni(OH)_2$ was obtained by cation exchange between $Ni(OH)_2$ and Cu^{2+}, and CuNi-$Ni(OH)_2$ nanoarray was obtained by reducing $Cu(OH)_2$-$Ni(OH)_2$ by $NaBH_4$. As shown in Fig. S12a, $Ni(OH)_2$ nanosheets grown neatly and vertically on the NF substrate, after Cu^{2+} exchange, the $Cu(OH)_2$ nanoparticles appeared on the top of the nanosheets (Fig. S12b). Finally, after reduction, the combination of CuNi alloy and $Ni(OH)_2$ nanosheets were obtained (Fig. S12c), which could be verified from the XRD spectrum (Fig. S13). However, as shown in Fig. S11d-f,

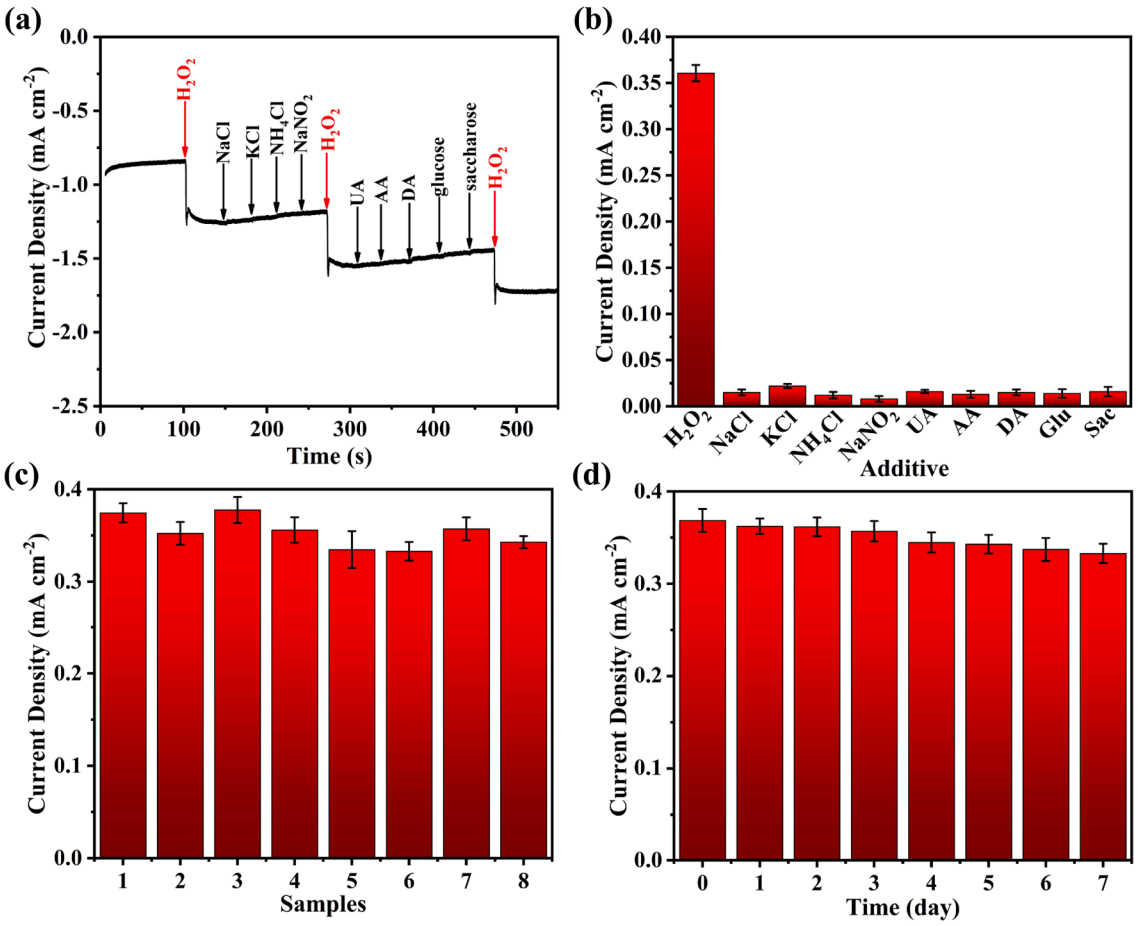

Fig. 6. (a) Amperometric response of CuCo-Cu@CoCH electrode to the addition of H_2O_2, NaCl, KCl, NH_4Cl, $NaNO_2$, UA, AA, glucose and saccharose at −0.25 V (vs. SCE) in 0.1 M PBS solution; (b) Amperometric response of CuCo-Cu@CoCH with various interferences; (c) The amperometric responses of 8 samples with the addition of 100 μM H_2O_2 at −0.25 V in 0.1 M PBS solution to test repeatability of CuCo-Cu@CoCH; (d) Amperometric responses of the electrodes with the injection of 100 μM H_2O_2 at–0.25 V in 0.1 M PBS solution (PH = 7), the test was made every day in a week to test the stability.

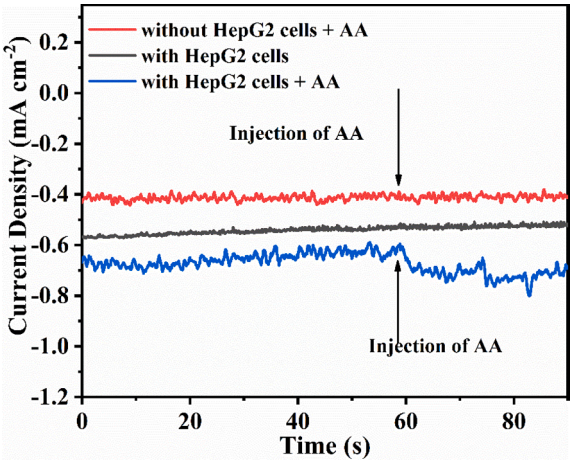

Fig. 7. Amperometric responses of CuCo-Cu@CoCH electrode to the addition of 5 mM AA with and without HepG2 cells as well as in the presence of HepG2 cells without AA at −0.25 V (vs. SCE) in N_2-saturated 0.1 M PBS solution.

pure $Ni(OH)_2$ nanoarray could not be reduced under the same solution.

3. Conclusions

In conclusion, a stamen-like CuCo-Cu@CoCH electrode was prepared by co-reduction with a large electrochemical surface active area and fast interfacial charge transfer. The electrode exhibited excellently in H_2O_2 detection with a sensitivity of 3570 μA mM^{-1} cm^{-2} (1 μM–100 μM) and 3290 μA mM^{-1} cm^{-2} (100 μM–2000 μM), and a low LOD of 0.97 μM. The electrode also had superior selectivity and stability, and could be used in detection of H_2O_2 released by HepG2 cells. The co-reduction method could also be used to prepare NiCu nanostructure, which might offer a novel solution to prepare nanostructure of alloy.

CRediT authorship contribution ststement

Ning Han: Writing – original draft. **Shiyu Hu:** Writing – original draft. **Liying Zhang:** Writing – original draft, Writing – review & editing. **Shasha Yi:** Writing – review & editing. **Zongtao Zhang:** Writing – review & editing. **Yu Wang:** Writing – review & editing. **Ying Zhou:** Writing – review & editing. **Deliang Chen:** Writing – review & editing. **Yanfeng Gao:** Writing – review & editing.

Declaration of Competing Interest

The authors declare that they have no known competing financial interests or personal relationships that could have appeared to influence the work reported in this paper.

Acknowledgment

This work was supported by the National Natural Science Foundation

of China (22002142).

Appendix A. Supplementary material

The detail of the materials and instruments and the preparation of CuCo-Cu@CoCH, CuNi-Ni(OH)$_2$, CoCH NWs, Ni(OH)$_2$ NSs,Cu@CoCH, Co@CoCH and CuCo/NF; the SEM images of CuCo-Cu@CoCH electrode with different time of ion exchange, CuNi-Ni(OH)$_2$, CoCH NWs and Ni(OH)$_2$ NSs; the XRD images of the CoCH was scraped off from the NF, CuNi-Ni(OH)$_2$, CoCH NWs and Ni(OH)$_2$ NSs; XPS spectra of C 1s of CuCo-Cu@CoCH; electrochemical characterization of CoCH, Cu@CoCH, Co@CoCH, CuCo/NF, Cu(OH)$_2$@CoCH and CuCo-Cu@CoCH. Supplementary data to this article can be found online at https://doi.org/10.1016/j.apsusc.2021.151879.

References

[1] D. Sun, D. Yang, P. Wei, B. Liu, Z. Chen, L. Zhang, J. Lu, One-Step Electrodeposition of Silver Nanostructures on 2D/3D Metal-Organic Framework ZIF-67: Comparison and Application in Electrochemical Detection of Hydrogen Peroxide, ACS Appl. Mater. Interfaces 12 (2020) 41960–41968.

[2] Z. Wang, F. Xie, Z. Liu, G. Du, A.M. Asiri, X. Sun, High-Performance Non-Enzyme Hydrogen Peroxide Detection in Neutral Solution: Using a Nickel Borate Nanoarray as a 3D Electrochemical Sensor, Chemistry 23 (2017) 16179–16183.

[3] H. Guan, Y. Zhao, J. Zhang, Y. Liu, S. Yuan, B. Zhang, Uniformly dispersed PtNi alloy nanoparticles in porous N-doped carbon nanofibers with high selectivity and stability for hydrogen peroxide detection, Sens. Actuat., B 261 (2018) 354–363.

[4] Y. Sun, M. Luo, Y. Qin, S. Zhu, Y. Li, N. Xu, X. Meng, Q. Ren, L. Wang, S. Guo, Atomic-Thick PtNi Nanowires Assembled on Graphene for High-Sensitivity Extracellular Hydrogen Peroxide Sensors, ACS Appl. Mater. Interfaces 9 (2017) 34715–34721.

[5] M. Peng, Y. Zhao, D. Chen, Y. Tan, Free-Standing 3D Electrodes for Electrochemical Detection of Hydrogen Peroxide, ChemCatChem 11 (2019) 4222–4237.

[6] H. Guan, J. Zhang, Y. Liu, Y. Zhao, B. Zhang, Rapid quantitative determination of hydrogen peroxide using an electrochemical sensor based on PtNi alloy/CeO_2 plates embedded in N-doped carbon nanofibers, Electrochim. Acta 295 (2019) 997–1005.

[7] Y. Li, K. Huan, D. Deng, L. Tang, J. Wang, L. Luo, Facile Synthesis of $ZnMn_2O_4$@rGO Microspheres for Ultrasensitive Electrochemical Detection of Hydrogen Peroxide from Human Breast Cancer Cells, ACS Appl. Mater. Interfaces 12 (2020) 3430–3437.

[8] N.S. Dumore, M. Mukhopadhyay, Sensitivity enhanced SeNPs-FTO electrochemical sensor for hydrogen peroxide detection, Electroanal. Chem. 878 (2020), 114544.

[9] N.V. Klassen, D. Marchington, H.C.E. McGowan, H_2O_2 Determination by the I_3^- Method and by $KMnO_4$ Titration, Anal. Chem. 66 (1994) 2921–2925.

[10] S.-A. Supharoek, K. Ponhong, W. Siriangkhawut, K. Grudpan, A new method for spectrophotometric determination of carbaryl based on rubber tree bark peroxidase enzymatic reaction, Microchem. J. 144 (2019) 56–63.

[11] M. Nasir, S. Rauf, N. Muhammad, M. Hasnain Nawaz, A. Anwar Chaudhry, M. Hamza Malik, S. Ahmad Shahid, A. Hayat, Biomimetic nitrogen doped titania nanoparticles as a colorimetric platform for hydrogen peroxide detection, J. Colloid Interface Sci. 505 (2017) 1147–1157.

[12] M. Haddad Irani-nezhad, A. Khataee, J. Hassanzadeh, Y. Orooji, A Chemiluminescent Method for the Detection of H_2O_2 and Glucose Based on Intrinsic Peroxidase-Like Activity of WS_2 Quantum Dots, Molecules 24 (2019) 689.

[13] H. Dai, Y. Chen, X. Niu, C. Pan, H. Chen, X. Chen, High-performance electrochemical biosensor for nonenzymatic H_2O_2 sensing based on Au@C-Co_3O_4 heterostructures, Bios. Bioelectron. 118 (2018) 36–43.

[14] R. Zhang, W. Chen, Recent advances in graphene-based nanomaterials for fabricating electrochemical hydrogen peroxide sensors, Bios. Bioelectron. 89 (2017) 249–268.

[15] S. Lee, Y.J. Lee, J.H. Kim, G.-J. Lee, Electrochemical Detection of H_2O_2 Released from Prostate Cancer Cells Using Pt Nanoparticle-Decorated rGO–CNT Nanocomposite-Modified Screen-Printed Carbon Electrodes, Chemosensors 8 (2020) 63.

[16] F. Zhao, S. Zhou, Y. Zhang, Ultrasensitive Detection of Hydrogen Peroxide Using Bi_2Te_3 Electrochemical Sensors, ACS Appl. Mater. Interfaces 13 (2021) 4761–4767.

[17] W. Chen, S. Cai, Q.-Q. Ren, W. Wen, Y.-D. Zhao, Recent advances in electrochemical sensing for hydrogen peroxide: a review, Analyst 137 (2012) 49–58.

[18] M. Baghayeri, M. Ghanei-Motlagh, R. Tayebee, M. Fayazi, F. Narenji, Application of graphene/zinc-based metal-organic framework nanocomposite for electrochemical sensing of As(III) in water resources, Anal. Chim. Acta 1099 (2020) 60–67.

[19] M. Baghayeri, A. Amiri, M. Fayazi, M. Nodehi, A. Esmaeelnia, Electrochemical detection of bisphenol a on a MWCNTs/$CuFe_2O_4$ nanocomposite modified glassy carbon electrode, Mater. Chem. Phys. 261 (2021), 124247.

[20] M. Liu, M. An, J. Xu, T. Liu, L. Wang, Y. Liu, J. Zhang, Three-dimensional carbon foam supported NiO nanosheets as non-enzymatic electrochemical H_2O_2 sensors, Appl. Surf. Sci. 542 (2021), 148699.

[21] Y. Nuevo Ordoñez, M. Montes-Bayón, E. Blanco-González, A. Sanz-Medel, Quantitative Analysis and Simultaneous Activity Measurements of Cu, Zn-Superoxide Dismutase in Red Blood Cells by HPLC−ICPMS, Anal. Chem. 82 (2010) 2387–2394.

[22] H. Ohtsu, Y. Shimazaki, A. Odani, O. Yamauchi, W. Mori, S. Itoh, S. Fukuzumi, Synthesis and Characterization of Imidazolate-Bridged Dinuclear Complexes as Active Site Models of Cu, Zn-SOD, J. Am. Chem. Soc. 122 (2000) 5733–5741.

[23] C. Cheng, C. Zhang, X. Gao, Z. Zhuang, C. Du, W. Chen, 3D Network and 2D Paper of Reduced Graphene Oxide/Cu_2O Composite for Electrochemical Sensing of Hydrogen Peroxide, Anal. Chem. 90 (2018) 1983–1991.

[24] A. Ngamaroonchote, Y. Sanguansap, T. Wutikhun, K. Karn-orachai, Highly branched gold–copper nanostructures for non-enzymatic specific detection of glucose and hydrogen peroxide, Microchim. Acta 187 (2020) 559.

[25] Z.M. Sheng, Z.Z. Gan, H. Huang, R.L. Niu, Z.W. Han, R.P. Jia, M-Nx (M = Fe Co, Ni, Cu) doped graphitic nanocages with High specific surface Area for non-enzymatic electrochemical detection of H2O2, Sens. Actuat., B 305 (2020), 127550.

[26] H.-B. Noh, K.-S. Lee, P. Chandra, M.-S. Won, Y.-B. Shim, Application of a Cu–Co alloy dendrite on glucose and hydrogen peroxide sensors, Electrochim. Acta 61 (2012) 36–43.

[27] J. Xie, D. Cheng, Z. Zhou, X. Pang, M. Liu, P. Yin, Y. Zhang, H. Li, X. Liu, S. Yao, Hydrogen peroxide sensing in body fluids and tumor cells via in situ produced redox couples on two-dimensional holey $CuCo_2O_4$ nanosheets, Microchim. Acta 187 (2020) 469.

[28] Q. Wang, D. Niu, J. Shi, L. Wang, A Three-in-one ZIFs-Derived CuCo(O)/GOx@PCNs Hybrid Cascade Nanozyme for Immunotherapy/Enhanced Starvation/Photothermal Therapy, ACS Appl Mater Interfaces 13 (2021) 11683–11695.

[29] D. Song, T. Li, Y.Y. Wei, Z.R. Xu, Controlled formation of porous $CuCo_2O_4$ nanorods with enhanced oxidase and catalase catalytic activities using bimetal-organic frameworks as templates, *Colloids Surf. B.* 188 (2020), 110764.

[30] S. Cui, S. Gu, Y. Ding, J. Zhang, Z. Zhang, Z. Hu, Hollow mesoporous $CuCo_2O_4$ microspheres derived from metal organic framework: A novel functional materials for simultaneous H_2O_2 biosensing and glucose biofuel cell, Talanta 178 (2018) 788–795.

[31] Y. Wu, L. Lu, Z. Yu, X. Wang, Electrochemical sensor based on the Mn_3O_4/CeO_2 nanocomposite with abundant oxygen vacancies for highly sensitive detection of hydrogen peroxide released from living cells, Anal. Methods 13 (2021) 1672–1680.

[32] H. Wu, K. Xiao, T. Ouyang, Z. Wang, Y. Chen, N. Li, Z.Q. Liu, Co-Cr mixed spinel oxide nanodots anchored on nitrogen-doped carbon nanotubes as catalytic electrode for hydrogen peroxide sensing, J. Colloid Interface Sci. 585 (2021) 605–613.

[33] H. Karimi-Maleh, M.L. Yola, N. Atar, Y. Orooji, F. Karimi, P. Senthil Kumar, J. Rouhi, M. Baghayeri, A novel detection method for organophosphorus insecticide fenamiphos: Molecularly imprinted electrochemical sensor based on core-shell Co_3O_4@MOF-74 nanocomposite, J. Colloid Interface Sci. 592 (2021) 174–185.

[34] H. Karimi-Maleh, Y. Orooji, F. Karimi, M. Alizadeh, M. Baghayeri, J. Rouhi, S. Tajik, H. Beitollahi, S. Agarwal, V.K. Gupta, S. Rajendran, A. Ayati, L. Fu, A. L. Sanati, B. Tanhaei, F. Sen, M. Shabani-Nooshabadi, P.N. Asrami, A. Al-Othman, A critical review on the use of potentiometric based biosensors for biomarkers detection, Bios. Bioelectron. 184 (2021), 113252.

[35] H. Karimi-Maleh, M. Alizadeh, Y. Orooji, F. Karimi, M. Baghayeri, J. Rouhi, S. Tajik, H. Beitollahi, S. Agarwal, V.K. Gupta, S. Rajendran, S. Rostamnia, L. Fu, F. Saberi-Movahed, S. Malekmohammadi, Guanine-Based DNA Biosensor Amplified with Pt/SWCNTs Nanocomposite as Analytical Tool for Nanomolar Determination of Daunorubicin as an Anticancer Drug: A Docking/Experimental Investigation, Ind. Eng. Chem. Res. 60 (2021) 816–823.

[36] Y. Orooji, P.N. Asrami, H. Beitollahi, S. Tajik, M. Alizadeh, S. Salmanpour, M. Baghayeri, J. Rouhi, A.L. Sanati, F. Karimi, An electrochemical strategy for toxic ractopamine sensing in pork samples; twofold amplified nano-based structure analytical tool, J. Food Meas. Charact. 15 (2021) 4098–4104.

[37] M. Nodehi, M. Baghayeri, H. Veisi, Preparation of GO/Fe_3O_4@PMDA/AuNPs nanocomposite for simultaneous determination of As^{3+} and Cu^{2+} by stripping voltammetry, Talanta 230 (2021), 122288.

[38] M. Baghayeri, A. Amiri, F. Karimabadi, S. Di Masi, B. Maleki, F. Adibian, A. R. Pourali, C. Malitesta, Magnetic MWCNTs-dendrimer: A potential modifier for electrochemical evaluation of As (III) ions in real water samples, Electroanal. Chem. 888 (2021), 115059.

[39] B. Li, L.-H. Liu, X.-F. Zhang, Y. Gao, Z.-P. Deng, L.-H. Huo, S. Gao, Echinus-like Cu–Mo_2C/C yolk-shell composites for ultrasensitive detection of hydrogen peroxide, Electrochim. Acta 373 (2021), 137908.

[40] Y. Zhu, K. Yan, Z. Xu, J. Wu, J. Zhang, Cathodic "signal-on" photoelectrochemical aptasensor for chloramphenicol detection using hierarchical porous flower-like Bi-BiOI@C composite, Bios. Bioelectron. 131 (2019) 79–87.

[41] Z.-H. Xue, H. Su, Q.-Y. Yu, B. Zhang, H.-H. Wang, X.-H. Li, J.-S. Chen, Janus Co/CoP Nanoparticles as Efficient Mott-Schottky Electrocatalysts for Overall Water Splitting in Wide pH Range, Adv. Energy Mater. 7 (2017) 1602355.

[42] C. Yu, J. Fu, M. Muzzio, T. Shen, D. Su, J. Zhu, S. Sun, CuNi Nanoparticles Assembled on Graphene for Catalytic Methanolysis of Ammonia Borane and Hydrogenation of Nitro/Nitrile Compounds, Chem. Mater. 29 (2017) 1413–1418.

[43] J. Li, Q.-L. Zhu, Q. Xu, Non-noble bimetallic CuCo nanoparticles encapsulated in the pores of metal–organic frameworks: synergetic catalysis in the hydrolysis of ammonia borane for hydrogen generation, Catal. Sci. Technol. 5 (2015) 525–530.

[44] B. He, H. Liu, Z. Lin, L. Yan, J. Ning, Y. Zhong, C. Zheng, Z. Zhang, Y. Hu, A new photocatalyst based on $Co(CO_3)_{0.5}(OH)\cdot 0.11H_2O/Bi_2WO_6$ nanocomposites for high-efficiency cocatalyst-free O_2 evolution, Chem. Eng. J. 359 (2019) 924–932.

[45] B. Yang, N. Han, L. Zhang, S. Yi, Z. Zhang, Y. Wang, Y. Zhou, D. Chen, Y. Gao, Cu_3Pt/Cu_2O nanorod array prepared by a facile method for glucose detection, Appl. Surf. Sci. 534 (2020), 147596.
[46] W. Sang, C. Wang, X. Zhang, X. Yu, C. Yu, J. Zhao, X. Wang, X. Yang, L. Li, Dendritic $Co_{0.52}Cu_{0.48}$ and $Ni_{0.19}Cu_{0.81}$ alloys as hydrogen generation catalysts via hydrolysis of ammonia borane, Int. J. Hydrogen Energ. 42 (2017) 30691–30703.
[47] M. Rahimi-Nasrabadi, H.R. Naderi, M.S. Karimi, F. Ahmadi, S.M. Pourmortazavi, Cobalt carbonate and cobalt oxide nanoparticles synthesis, characterization and supercapacitive evaluation, J. Mater. Sci-Mater. El. 28 (2016) 1877–1888.
[48] S. Sun, X. Zhang, Y. Sun, S. Yang, X. Song, Z. Yang, Hierarchical CuO nanoflowers: water-required synthesis and their application in a nonenzymatic glucose biosensor, Phys. Chem. Chem. Phys. 15 (2013) 10904–10913.
[49] H. Gu, Q. Zhong, Y. Zeng, S. Zhang, Y. Bu, Ni and Zn co-substituted $Co(CO_3)_{0.5}OH$ self-assembled flowers array for asymmetric supercapacitors, J. Colloid Interface Sci. 573 (2020) 299–306.
[50] G. Zhang, P. Qin, R. Nasser, S. Li, P. Chen, J. Song, Synthesis of $Co(CO_3)_{0.5}(OH)/Ni_2(CO_3)(OH)_2$ nanobelts and their application in flexible all-solid-state asymmetric supercapacitor, Chem. Eng. J. 387 (2020), 124029.
[51] J.R. Deka, D. Saikia, N.-F. Lu, K.-T. Chen, H.-M. Kao, Y.-C. Yang, Space confined synthesis of highly dispersed bimetallic CoCu nanoparticles as effective catalysts for ammonia borane dehydrogenation and 4-nitrophenol reduction, Appl. Surf. Sci. 538 (2021), 148091.
[52] J. Huang, Q. Hu, X. Guo, Q. Zeng, L. Wang, Rethinking $Co(CO_3)_{0.5}(OH)\cdot 0.11H_2O$: a new property for highly selective electrochemical reduction of carbon dioxide to methanol in aqueous solution, Green Chem. 20 (2018) 2967–2972.
[53] B. Li, L.H. Liu, X.F. Zhang, Y. Gao, Z.P. Deng, L.H. Huo, S. Gao, Novel neuron-network-like Cu-MoO_2/C composite derived from bimetallic organic framework for highly efficient detection of hydrogen peroxide, Anal. Chim. Acta 1143 (2021) 73–83.
[54] C. Zhao, H. Zhang, J. Zheng, A non-enzymatic electrochemical hydrogen peroxide sensor based on Ag decorated boehmite nanotubes/reduced graphene oxide nanocomposites, Electroanal. Chem. 784 (2017) 55–61.
[55] A. Mohammad, M.E. Khan, T. Yoon, M. Hwan Cho, Na,O-co-doped-graphitic-carbon nitride (Na,O-g-C_3N_4) for nonenzymatic electrochemical sensing of hydrogen peroxide, Appl. Surf. Sci. 525 (2020) 146353.
[56] Z. Duan, C. Huang, X. Yang, A. Hu, X. Lu, Q. Jiang, Preparation of SnS_2/MWCNTs chemically modified electrode and its electrochemical detection of H_2O_2, Anal Bioanal Chem. 412 (2020) 4403–4412.
[57] L. Yang, C. Xu, W. Ye, W. Liu, An electrochemical sensor for H_2O_2 based on a new Co-metal-organic framework modified electrode, Sens. Actuat., B 215 (2015) 489–496.
[58] C. Xu, F. Sun, H. Gao, J. Wang, Nanoporous platinum-cobalt alloy for electrochemical sensing for ethanol, hydrogen peroxide, and glucose, Anal. Chim. Acta 780 (2013) 20–27.
[59] M. Annalakshmi, S. Kumaravel, S.-M. Chen, T.-W. Chen, Thermo-regulated synthesis of NiMn layered double hydroxides for real-time determination of hydrogen peroxide in living cells and oxidase activity, Appl. Surf. Sci. 539 (2021), 148256.
[60] X. Sun, S. Guo, Y. Liu, S. Sun, Dumbbell-like PtPd-Fe_3O_4 nanoparticles for enhanced electrochemical detection of H_2O_2, Nano Lett. 12 (2012) 4859–4863.
[61] M.A. Rashed, M. Faisal, F.A. Harraz, M. Jalalah, M. Alsaiari, S.A. Alsareii, A Highly Efficient Nonenzymatic Hydrogen Peroxide Electrochemical Sensor Using Mesoporous Carbon Doped ZnO Nanocomposite, J. Electrochem. Soc. 168 (2021), 027512.
[62] D.M. Nguyen, H.N. Bich, P.D. Hai Anh, P.H. Ai-Le, Q.B. Bui, Vertical copper oxide nanowire arrays attached three-dimensional macroporous framework as a self-supported sensor for sensitive hydrogen peroxide detection, Arab. J. Chem. 13 (2020) 3934–3945.
[63] L. Zhang, F. Yuan, X. Zhang, L. Yang, Facile synthesis of flower like copper oxide and their application to hydrogen peroxide and nitrite sensing, Chem. Cent. J. 5 (2011) 75.
[64] B. Patella, M. Buscetta, S. Di Vincenzo, M. Ferraro, G. Aiello, C. Sunseri, E. Pace, R. Inguanta, C. Cipollina, Electrochemical sensor based on rGO/Au nanoparticles for monitoring H_2O_2 released by human macrophages, Sens. Actuat., B 327 (2021), 128901.
[65] L. Kong, Z. Ren, N. Zheng, S. Du, J. Wu, J. Tang, H. Fu, Interconnected 1D Co_3O_4 nanowires on reduced graphene oxide for enzymeless H_2O_2 detection, Nano Res. 8 (2015) 469–480.
[66] S.H. Wu, X.B. Huang, Y. Tang, L.M. Ma, Y. Liu, J.J. Sun, Temperature controllable electrochemical sensors based on horseradish peroxidase as electrocatalyst at heated Au disk electrode and its preliminary application for H_2O_2 detection, Anal. Chim. Acta 1096 (2020) 44–52.
[67] A. Arjunan, A. Sukeri, D.P.M. Saraiva, P.B. Miranda, M. Bertotti, Electrochemical Studies of Hydrogen Peroxide Oxidation on a Nanoporous Gold Surface: Fundamental and Analytical Applications, J. Electrochem. Soc. 167 (2020).
[68] F. Mollarasouli, S. Kurbanoglu, K. Asadpour-Zeynali, S.A. Ozkan, Non-enzymatic monitoring of hydrogen peroxide using novel nanosensor based on $CoFe_2O_4$@CdSeQD magnetic nanocomposite and rifampicin mediator, Anal. Bioanal. Chem. 412 (2020) 5053–5065.
[69] B. Yang, N. Han, S. Hu, L. Zhang, S. Yi, Z. Zhang, Y. Wang, D. Chen, Y. Gao, Cu/ZnO Nano-Thorn with Modifiable Morphology for Photoelectrochemical Detection of Glucose, J. Electrochem. Soc. 168 (2021), 027516.
[70] Y. Yuan, X. Chen, X. Zhang, Z. Wang, R. Yu, A MOF-derived CuCo(O)@carbon–nitrogen framework as an efficient synergistic catalyst for the hydrolysis of ammonia borane, Inorg. Chem. Front. 7 (2020) 2043–2049.